



Parameterization of proximal humerus locking plate impingement with in vitro, in silico, and in vivo techniques

Emily M. Bachner, BAS^a, Elaine C. Schmidt, MS^a, Matthew Chin, BS^a,
Surena Namdari, MD^{a,b}, Josh R. Baxter, PhD^c, Michael W. Hast, PhD^{a,*}

^aBiedermann Laboratory for Orthopaedic Research, Department of Orthopaedic Surgery, University of Pennsylvania, Philadelphia, PA, USA

^bDepartment of Orthopaedic Surgery, Rothman Institute at Thomas Jefferson University, Philadelphia, PA, USA

^cHuman Motion Lab, Department of Orthopaedic Surgery, University of Pennsylvania, Philadelphia, PA, USA

Background: Locked plating of displaced proximal humeral fractures is common, but rates of subacromial impingement remain high. This study used a multidisciplinary approach to elucidate the relationships between common surgical parameters, anatomic variability, and the likelihood of plate impingement.

Methods: The experiment was completed in 3 phases. First, a controlled in vitro experiment was conducted to simulate impingement. Second, a dynamic in silico musculoskeletal model modeled changes to implant geometry, surgical techniques, and acromial anatomy, where a collision detection algorithm was used to simulate impingement. Finally, in vivo shoulder kinematics were recorded for 9 activities of daily living. Motions that created a high likelihood of impingement were identified.

Results: Of simulated impingement events, 73.9% occurred when the plate was moved proximally, and 84% occurred when acromial tilt was 20° or 25°. Simulations of impingement occurred at cross-body adduction angles between 10° and 50°. Impingement occurred at an average of $162.0^\circ \pm 14.8^\circ$ abduction with 10 mm distal plate placement, whereas the average was $72.1^\circ \pm 11.4^\circ$ with 10 mm proximal placement. A patient may encounter these shoulder angles when performing activities such as combing one's hair, lifting an object overhead, and reaching behind one's head.

Discussion and Conclusion: Proximal implant placement and decreases in acromial tilt play major roles in the likelihood of impingement, whereas plate thickness and humeral head center of rotation should also be considered. Careful preoperative planning that includes these factors could help guide operative decision making and improve clinical outcomes.

Level of evidence: Basic Science Study; Biomechanics and Kinesiology

© 2018 Journal of Shoulder and Elbow Surgery Board of Trustees. All rights reserved.

Keywords: Proximal humerus; locked plate; impingement; biomechanics; cadaveric; computational model

The University of Pennsylvania approved this human study (approval: 824466).

*Reprint requests: Michael W. Hast, PhD, Biedermann Laboratory for Orthopaedic Research, Orthopaedic Surgery, University of Pennsylvania, 3737 Market St, Ste 1050, 10th Flr, Philadelphia, PA 19104, USA.

E-mail address: hast@pennmedicine.upenn.edu (M.W. Hast).

Proximal humeral fractures have become the third most common fracture type in patients aged older than 65^{4,22,31,34} and are expected to increase 3-fold over the next 30 years.¹ The development of locking plate technology for proximal humeral fracture fixation has become increasingly used and

widely accepted, particularly for patients with osteoporotic bone.² Unfortunately, reported complication rates are high, ranging from 20% to 49% in some studies.^{8,11,30}

Impingement between the acromion and the proximal portion of a locking plate is believed to be a potential source of pain that may also limit the patient's range of motion. Preventing postoperative subacromial impingement is especially difficult due to wide variability in shoulder joint morphology within humans.²⁴ One study reported that 42.4% of patients opted to remove hardware because of impingement-related issues.²¹

Previous studies have suggested that proximal positioning of the plate may lead to impingement,^{5,32} and there are many reasonable causes for such a scenario. Proximal plate repositioning may be due to slight errors in surgical technique, purposeful positioning to optimize fixation, or as a result of small humeral anatomy paired with a single-sized implant. To date, no studies have attempted to biomechanically quantify "how high is too high?" or have provided quantifiable guidelines with respect to implant design, shoulder anatomy, and desired range of motion when considering subacromial impingement.

The goal of this study was to use a multidisciplinary approach to elucidate the relationships between common surgical parameters, anatomic variability, and the likelihood of plate impingement. The study used a combination of in vitro, in silico, and in vivo models to characterize postoperative function of the joint. Accurate estimations of surgical impingement, caused by changes in surgical and anatomic parameters, will help provide clarity on this complicated issue.

Materials and methods

This experiment was performed in 3 phases (Fig. 1). First, a controlled dynamic cadaveric model was created to record impingement events during simple abduction motions.

Second, a computational musculoskeletal model of the upper extremity was used to identify the onset of subacromial impingement. This model was previously validated by comparing in vivo kinematics

to predictions of upper extremity motions using electromyogram-based and optimization-based control signals.²⁹ In this computational setting, a series of controlled abduction motions were simulated while variables of plate placement, plate thickness, acromial geometry, and humerus center of rotation (COR) were systematically changed.

Third, kinematics associated with 9 activities of daily living (ADLs) in healthy individuals were recorded with 3-dimensional (3-D) motion capture. Shoulder joint angles were compared against simulation outputs, and high-risk ADLs were identified.

Phase 1—in vitro experiment

This study used 4 cadaveric upper extremities (2 men, 2 women; mean age, 66.75 years). Shoulder joints were isolated, and the humerus was amputated at the midshaft. A deltoid-splitting approach was used, and an incision was made from the tip of the acromion distally to the midpoint of the humerus. The deltoid muscles were transected, and the subacromial bursa was excised to provide gross exposure of the proximal humerus. This model represented a passive motion, and therefore, no tension or forces were applied to any muscles in the system.

The distal humerus was potted in polycarbonate tubing with polymethyl methacrylate (Lang Dental, Wheeling, IL, USA). Locking plates (Philos; DePuy Synthes, Warsaw, IN, USA) were securely fixed on the humeri according to the manufacturer's guidelines with 2 bicortical screws (3.5-mm diameter, 35-mm length).¹⁰ A fracture was not simulated, and no screws were inserted into the humeral head, because this study focused solely on impingement and not fixation strength. The plate was visually confirmed to sit flush to the proximal humerus, which was reconfirmed with fluoroscopic images (SIREMOBIL Compact (L) C-Arm; Siemens, Washington, DC, USA) which were taken in anterior/posterior and medial/lateral outlet views.

Post hoc measurements were made with ImageJ (National Institutes of Health, Bethesda, MD, USA) and MATLAB (MathWorks, Natick, MA, USA) software for humeral head radii, acromial tilt (the angle between the anteroinferior edge of the acromion, posteroinferior edge of the acromion, and the inferior tip of the coracoid process), and acromial slope (the supplement of the angle between the posteroinferior edge, the inferior aspect, and anteroinferior edge the acromion; [Supplementary Fig. S1](#)).²⁴

Several preparatory steps were required to track joint kinematics and detect subacromial impingement in real time. For the purpose

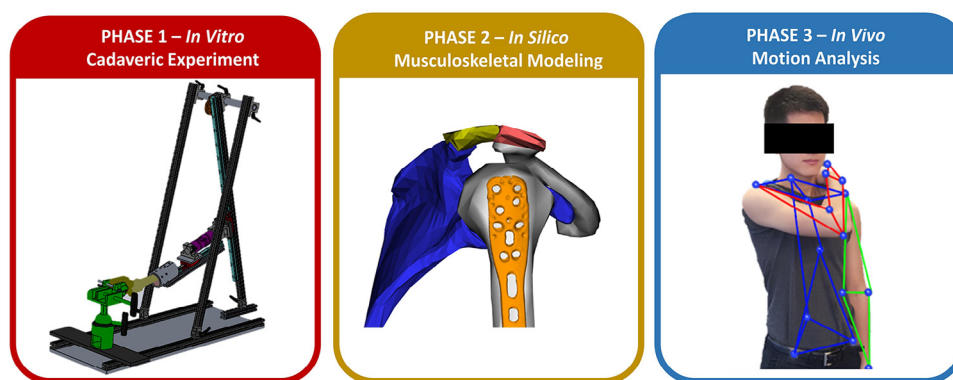


Figure 1 A workflow diagram outlining the methods used to perform the study. Impingement events were recorded during simple abduction motions in phase 1. Computational simulations of prescribed motions with systematically changing variables were made in phase 2. Phase 3 used motion capture techniques to compare shoulder joint angles during activities of daily living to those output in phase 2.

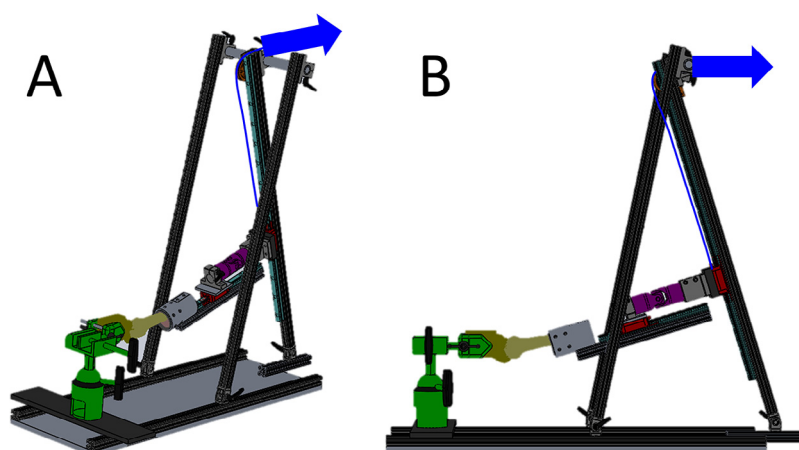


Figure 2 Computer-aided drawings of the custom jig built for the experiment in (A) isometric and (B) side views. The scapulae were held in place with a scapula clamp attached to a vise (green). Two sleds (red) were attached to one another with a universal joint (magenta), and the sleds were allowed to freely translate on linear tracks (teal). Displacement of the rope (blue) created an abduction motion that was controlled by a rotational actuator of a universal test frame (not shown).

of motion capture, retroreflective marker clusters were rigidly attached to the plate and scapula. Thin-film pressure sensors (iScan 6900; Tekscan, Inc., South Boston, MA, USA) were covered with a patch of cellophane tape that extended beyond the boundaries of the sensor. Beaded Kirschner wires were inserted through the tape and into the proximal portion of the humerus, such that the sensor consistently covered the proximal aspect of the plate during motions (Supplementary Fig. S2).

Simulations of abduction were created with a custom-built jig (Fig. 2). Scapulae were held stable with a scapula clamp (Pacific Research Laboratories, Vashone, WA, USA) and a vise. The potted distal humeri were fixed to a sled that allowed free translation on a low-friction linear bearing. This assembly was attached to a second sled via a universal joint. The second sled was allowed to translate on a linear bearing that was angled 60° relative to horizontal. A rope and pulley connected the sled to the rotational actuator of a universal test frame (ElectroForce 3550; TA Instruments, New Castle, DE, USA). Initial shoulder angles were controlled by rotating the scapula in the vise and clamping down to achieve a static pose of approximately 30° abduction. Dynamic simulations of 20° of abduction were performed in 5 seconds. If impingement did not occur, adjustments were made to the initial scapular position in approximately 20° increments until an impingement event was created.

Scapular and humeral motions were tracked in real time using a 6-camera motion capture system (Optitrack; NaturalPoint, Inc., Corvallis, OR, USA) calibrated to 0.2 mm accuracy. Five anatomic points on the scapula were identified with an instrumented wand during static trials so that the post hoc computational model could be properly scaled (Supplementary Fig. S3). Motions of the marker clusters were recorded as the shoulder was abducted until impingement occurred.

To determine scapulohumeral joint angles, simplified representations of each cadaveric humerus and scapula were created in a simple 2-body, 6-degree-of-freedom, OpenSim model.⁹ The on-board geometry files of the humerus and scapula were scaled to represent the cadaveric specimens (See Appendix SA for details). A 3-D rendering of the locking plate was created by performing an optical 3-D scan (Afinia Einscan; Afinia, Chanhassen, MN, USA). The virtual plate was placed on the humerus in the model according

to the manufacturer's guidelines and held in place with a weld joint. Anatomic coordinate frames were assigned to the humerus and scapula, and marker trajectories were tracked with the inverse kinematics algorithm. The relative 3-D motions between the virtual humerus and scapula were characterized as a function of time. The timed data from the pressure sensor measurements were synchronized with the marker trajectory data, and initiation of impingement was identified by distinct increases in compressive forces.

Phase 2—in silico experiment

A validated computational model using the anthropometry of the upper extremity of a 50th percentile man¹² was adapted for this phase of the experiment.²⁹ Use of this model permitted the simulation of motions that are not easily recreated in a cadaveric setting and provided the ability to make systematic and controlled changes to other variables of interest. Shoulder kinematics were defined using a validated spherical coordinate system.¹⁷ This mechanical convention ensures the smooth execution of complex shoulder motions but uses nomenclature that is substantially different from clinical standards. For the purpose of clarity, results are described in the clinically relevant terms of cross-body adduction (humeral motion in the transverse plane) coupled with abduction (humeral elevation in the coronal plane).

Surgical and anatomic variables were introduced into the model to identify possible impingement events (Fig. 3). First, the plate was positioned neutrally according to the manufacturer's guidelines (8 mm distal to the rotator cuff attachment on the upper edge of the greater tuberosity).¹⁰ Position of the plate relative to the humerus was varied from the neutral location using 2 parameters: (1) proximal-distal displacements (−10 to +10 mm in 5-mm increments) and (2) plate thickness of 0 mm to represent natural bone as a control, 2.5 mm to represent the approximate thickness of the plate used in the study, and 5.0 mm to represent plates that may be thicker. A 0-mm thickness was used to represent natural bone because the model was programmed to detect contact between plate and bone, not bone and bone. Acromial tilt and slope were changed between 20° and 35° in 5° increments. Finally, the humeral head COR ranged from neutral

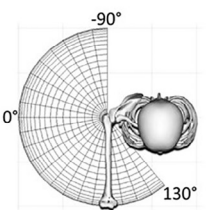
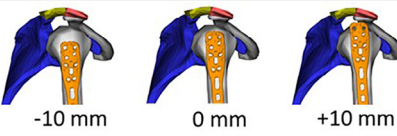
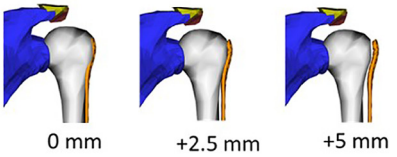

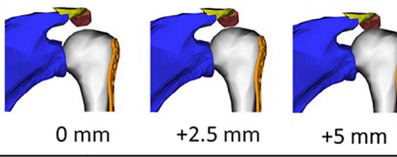
Independent Variables		Number of Variations
Cross-Body Adduction		23
Distal/Proximal Plate Position		5
Plate Thickness		3
Acromial Geometry		
	Tilt: 35° → 20°	4
	Slope: -20° → -35°	4
Humerus COR		3
Total Number of Simulations:		16,560

Figure 3 A diagram outlining the combinations of simulations that were performed with the in silico model.

to +5.0 mm proximal in 2.5-mm increments. This step was performed because the model uses a joint that does not translate during motions. Moving the COR proximally, relative to the scapula, represents translations that may occur during a motion.⁷

We executed 23 unique simulations to cover the entire range of motion of the shoulder joint (Fig. 3). For each simulation, the initial cross-body adduction angle was systematically adjusted from -90° to 130° in 10° increments. With this pose established, the arm was lowered to 0° abduction and raised to 180° . The on-board OpenSim elastic foundation contact algorithm was used to detect impingement between the plate and the acromion. Shoulder joint angles were recorded at the moment these collisions occurred. Results were pooled, and the parameters that were present during impingement were identified.

Phase 3—in vivo experiment

We recruited 8 healthy young individuals (4 men and 4 women; mean age, 21.5 years) with no history of shoulder injuries or pain who performed 9 commonly performed ADLs²⁶ (Table I) after providing

Table I Activities of daily living that were performed and simulated in the study

1	Place hand behind one's head with the elbow held straight out to the side
2	Comb hair
3	Reach the small of one's back to tuck in one's shirt with one's hand
4	Wash the back of the opposite shoulder
5	Wash the middle of one's back
6	Place a can of soup on a shelf at shoulder level without bending the elbow
7	Place a can of soup on an overhead shelf without bending the elbow
8	Place a 1-gallon container (3.6-4.5 kg) on a shelf at shoulder level without bending the elbow
9	Place a 1-gallon container on an overhead shelf without bending the elbow

written informed consent. These 9 tasks were selected from the functional assessment section of the American Shoulder and Elbow Surgeons Shoulder Score,²⁸ the Penn Shoulder Score,²³ and the Simple Shoulder Test.¹⁸ Upper extremity kinematics were measured using a 12-camera motion capture system (Raptor Series; Motion Analysis Corp., Santa Rosa, CA, USA). Reflective markers (9.5 mm; B&L Engineering, Santa Ana, CA, USA) were adhered bilaterally using skin-safe tape covering the seventh cervical vertebra, sternum, acromion, elbow epicondyles, and ulnar and radial styloid processes.

Participants stood upright with their arms straight and shoulders at 90° abduction and external rotation to scale the subject-specific musculoskeletal models. Marker labeling was visually confirmed, gaps were filled using cubic-spline interpolation, and marker trajectories were filtered. Shoulder kinematics were calculated using the same musculoskeletal model used in phase 2. Analysis of the root mean squared, total squared, and maximum error indicated that this model created was a good representation of the experimental kinematics. A boot-strapping technique was used to calculate 95% confidence intervals for elevation angle, abduction, and internal rotation for each ADL. Results were compared against computational predictions of impingement based on joint angle.

Results

Phase 1—cadaveric experiment

The cadaveric experiment measures were made in terms of scapulohumeral angulation. Simulated impingement occurred at a mean cross-body adduction angle of $22.1^\circ \pm 10.1^\circ$, abduction angle of $73.3^\circ \pm 14.5^\circ$, and external rotation of $26.7^\circ \pm 13.4^\circ$. Mean humeral head radii were 23.1 ± 2.4 mm. Acromial geometry identified using fluoroscopic imaging showed a mean acromial tilt of $26.2^\circ \pm 3.3^\circ$ and an acromial slope of $27.6^\circ \pm 5.7^\circ$.

Phase 2—computational model

Computational output measures were made in terms of thoracohumeral angles, and impingement only occurred when cross-body adduction angles were set between 10° and 50° for all trials (Table II, Figs. 4 and 5). More than 1 in 10 simulations exhibited impingement within this range of motion (368 of 3600 simulations). Bone-plate contact occurred at an

average of 162.0° abduction when the plate was placed 10 mm distally, and this initial angle of impingement steadily decreased as the plate was moved proximally, with a final average of 72.1° with 10 mm proximal placement. Although impingement is possible when the plate is placed distally (18.4%), 73.9% of impingement events occurred when the plate was moved proximally beyond the neutral location. Similarly, increases in plate thickness led to increases in impingement events (Table III).

Decreases in acromial tilt led to higher rates of impingement, with 84% of impingement events occurring when tilt was set to 20° or 25° (Table III, Fig. 5). Changes in the acromial slope had no effect on the likelihood of impingement.

Finally, proximal shifts of the humeral head COR also led to increases in impingement (Table III). For the sake of simplicity, these results are presented on a variable-by-variable basis, but complex relationships exist within this data set. More information regarding these relationships is available in [Supplementary Appendix SB](#).

Phase 3—in vivo motion comparison

Of the 9 ADLs that were recorded, only 3 motions produced shoulder kinematics in which impingement occurred within the model. Comparisons between the in silico and in vivo data revealed that reaching behind the head, lifting a light object overhead, and combing hair are activities with a high likelihood of impingement (Fig. 6). The other motions (lifting light and heavy objects to shoulder height, lifting heavy objects overhead, washing the opposite shoulder, washing the middle of one's back, and tucking in one's shirt) created joint angle combinations that did not create impingement in the simulations. There were no notable differences when comparing joint angle kinematics between sexes ([Supplementary Fig. S4](#)).

Discussion

This study improves the biomechanical understanding of locking plate-subacromial impingement, and the findings compare favorably to previous in vivo and in vitro studies. A previous cadaveric experiment measured an average

Table II Average values of variables of interest with relation to implant placement

Plate height (mm)	Instances of contact (%)	Cross-body abduction (°)	Thoracohumeral abduction (°)	Plate thickness (mm)	Acromial tilt (°)	Humerus COR (mm)
-10	13.0	39.2 ± 7.9	162.0 ± 14.8	4.4 ± 1.1	22.1 ± 3.2	4.6 ± 1.0
-5	5.4	38.0 ± 8.4	141.6 ± 22.9	5.0 ± 0.0	22.0 ± 2.7	5.0 ± 0.0
0	7.6	31.4 ± 6.9	102.6 ± 11.1	4.6 ± 0.9	21.4 ± 2.4	4.6 ± 0.9
5	18.5	29.4 ± 7.5	83.8 ± 8.4	4.1 ± 1.5	22.6 ± 3.6	4.4 ± 1.1
10	55.4	29.6 ± 10.2	72.1 ± 11.4	3.6 ± 1.8	24.3 ± 4.6	3.9 ± 1.6

COR, center of rotation.

Continuous data are presented as the mean \pm standard deviation.

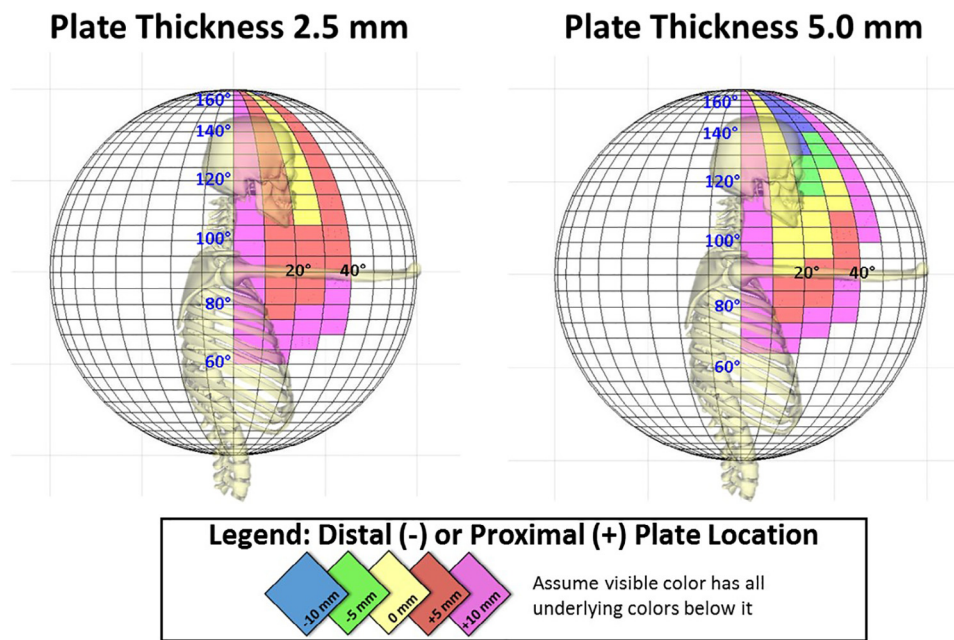


Figure 4 Sagittal view of the hemispherical shoulder joint range of motion for cross-body abduction (*black numbers*) and abduction (*blue numbers*). The *color maps* represent the range of motion that may be limited due to subacromial impingement. These plots show the changes that occur as a function of plate thickness and plate location. Humeral head center of rotation (+5 mm) and acromial tilt (20°) are held constant.

Table III Breakdown of computational model results showing the number of impingement events per modified parameter

Implant position		Implant thickness		Acromial tilt		Acromial slope		Humerus COR	
Variable	Events	Variable	Events	Variable	Events	Variable	Events	Variable	Events
-10 mm	48	0 mm	32	20°	192	-20°	92	0 mm	16
-5 mm	20	+2.5 mm	92	25°	116	-25°	92	+2.5 mm	84
0 mm	28	+5 mm	244	30°	48	-30°	92	+5 mm	268
+5 mm	68			35°	12	-35°	92		
+10 mm	204								

COR, center of rotation.

glenohumeral impingement angle of $74^\circ \pm 15^\circ$,²⁰ which is very similar to the overall average of $73.3^\circ \pm 14.5^\circ$ found in phase 1 of this experiment.

Results from the computational model matched well with static magnetic resonance imaging studies that investigated changes in subacromial space.¹³⁻¹⁵ Dynamic evaluations of subacromial impingement using open magnetic resonance imaging techniques found impingement at 93.5° of thoracohumeral abduction in asymptomatic patients.³³ This *in vivo* outcome matches well with the $92.0^\circ \pm 34.0^\circ$ simulated in the current study. The computational analysis in phase 2 used a generalized 50th percentile male model. The use of this size provided a reasonable approximation of human anatomy, based on the small number of cadaveric specimens used in phase 1. Specifically, the radius of the humeral head (23.5 mm) and the ranges of acromial slopes and tilts (20°-35°) fell within the range of the measurements taken in the cadaveric specimens (23.1 ± 2.4 mm, $27.6^\circ \pm 5.7^\circ$, and $26.2^\circ \pm 3.3^\circ$, respectively).

Differences between the cadaveric model and the computational model can be attributed to the use of scapulohumeral angles in the cadaveric model (due to a lack of a thorax), whereas thoracohumeral angles were used in the *in silico* and *in vivo* models. It is tempting to believe that the higher abduction angles observed in the computational model indicate a later onset of impingement. Interestingly, the opposite is true. When the scapular rhythm is accounted for, the mean scapulohumeral joint angles (73.3° abduction and 22.1° cross-body adduction) occur when the arm is positioned at approximately 118° of thoracohumeral abduction and 40° cross-body adduction (Fig. 7). This overapproximation of thoracohumeral impingement joint kinematics in the cadaveric model is likely due to a lax capsule, which may have caused the humeral head to move posteriorly relative to the glenoid.

The cadaveric jig developed in this experiment is unique. Existing abduction simulators often consist of a large, custom-made, semicircular ring to guide abduction motions.^{3,19} This

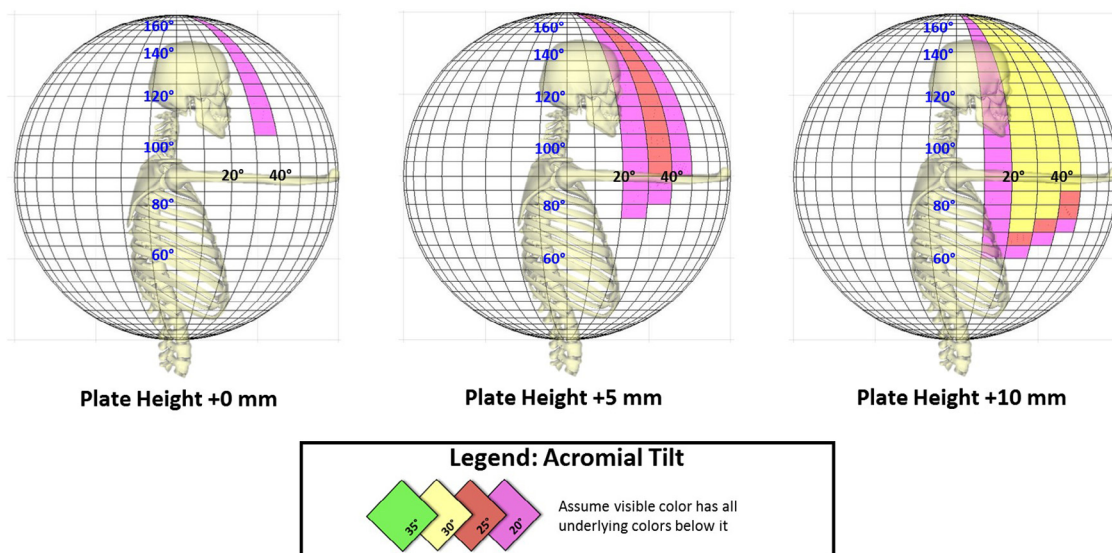


Figure 5 The changes in impingement that occur as a function of plate height and acromial tilt. Humeral head center of rotation (+5 mm) and plate thickness (2.5 mm) are held constant.

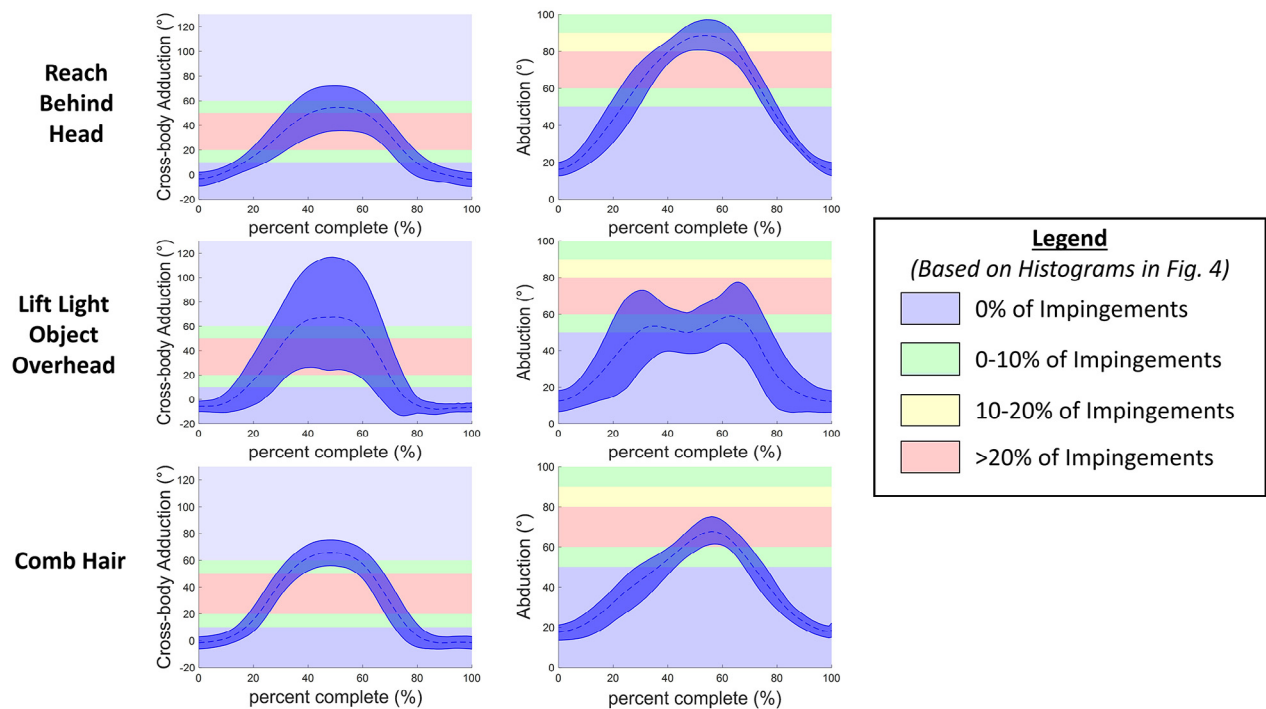


Figure 6 Plots of cross-body adduction and abduction during activities of daily motion. Mean values for all participants (*blue dashed*) and ± 1 standard deviation (*blue cloud*) are shown. Plots are overlaid on backgrounds that are colored to represent the number of impingements reported in the histograms in Supplementary Fig. S5.

existing design provides the ability to simulate muscle-driven motions over large ranges of motion; however, it also makes the rig both expensive and cumbersome. The rig developed in the current study provides a smooth and continuous shoulder motion. The range of motion can be changed by re-orienting the scapula at the beginning of a test. The created motions are passive in nature, and the weight of the sled must be considered. This rig was developed with linear, off-the-

shelf, components for less than \$1000 and can fold down to size for easy storage.

The musculoskeletal model developed in this study is also noteworthy. A variety of previous shoulder simulators have been developed to estimate muscle loads during motions and to investigate implant stresses and strains.^{6,16,27,35} To our knowledge, this model represents the first attempt to create a model that is tailored specifically to change surgical and anatomic

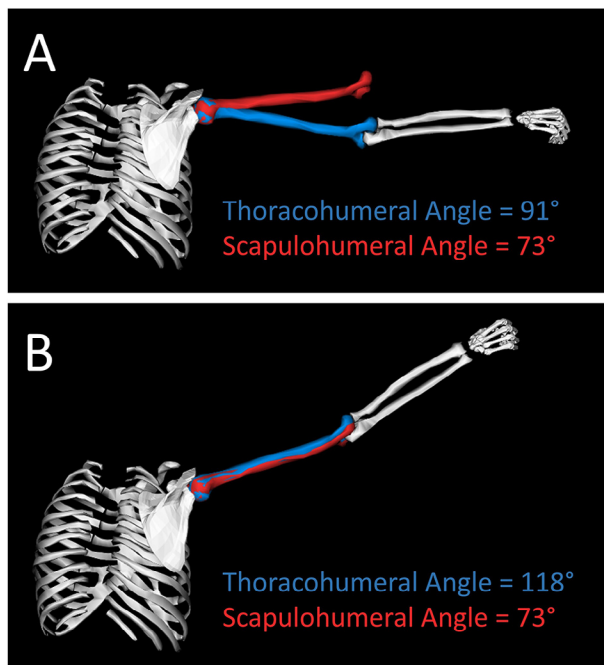


Figure 7 (A) Images from a musculoskeletal model that superimposes results from cadaveric (*red*) and computational (*blue*) models when the scapular rhythm is not simulated. (B) When scapular rhythm is accounted for, the arm must be in approximately 118° of thoracohumeral abduction to achieve 73° of glenohumeral abduction.

variables related to locking plate impingement. Changes to 4 of the 5 anatomic and surgical variables resulted in differences in subacromial impingement timing.

Interestingly, changes to acromial slope did not have an effect on the model. As mentioned previously, the acromial slope is determined by calculating the supplement of the angle between the posteroinferior edge, the inferior aspect, and anteroinferior edge the acromion. To make an adjustable acromial slope within the model, a “hinge joint” was placed at the inferior aspect of the acromion. Post hoc analysis of simulation outputs show that collisions between the plate and the acromion always occurred in the area posterior to the location of this “joint.”

This experiment has several limitations. The cadaveric simulations represent only passive motions and were not driven by coordinated muscle activations. Changes to the model’s basic bony geometry may alter simulation results. Because the subacromial space is relatively small, even a subtle change in any one of these variables could potentially result in changes to the onset of impingement. This is important to keep in mind, given that subacromial space dimensions are highly variable due to factors including sex, muscle activity, acromion morphology, posture, and age.^{13,25}

Aside from translating the humeral head COR, translations in the glenohumeral joint were constrained, which may not fully characterize the human condition. Simulation output suggests that impingement does not appear to be sensitive to

variation in acromial slope. However, a previous study compared patients with impingement syndrome to controls and found no significant difference in acromial slope between the 2 groups.²⁴ Therefore, this finding may have clinical relevance, and this topic requires further investigation.

Movement biomechanics may differ between patients after a surgical repair of a proximal humeral fracture and the healthy young adults with no history of upper extremity injury who participated in this study. Specifically, patients who experience impingement may adapt a greater degree of scapulothoracic mobility as a compensatory mechanism compared with healthy controls. However, the framework of this study supports the concepts that patient anatomy, surgical placement, and hardware parameters all can affect subacromial impingement risks.

Conclusion

Open reduction and internal fixation of proximal humeral fractures has relatively high complication rates, some of which can be attributed to subacromial impingement. Results from this experiment suggest that patient anatomy in conjunction with implant characteristics could help guide operative decision making. This study successfully implemented a multidisciplinary workflow that used in vitro biomechanical experimentation, in silico musculoskeletal modeling, and in vivo 3-D motion capture to quantify subacromial impingement. Results from this experiment confirm the importance of accounting for scapular rhythm and glenohumeral stability when simulating impingement. The data from the current experiment provide valuable information to clinicians and rehabilitative specialists to better predict patient outcomes and guide rehabilitation. Future studies within patient populations may help predict the likelihood of subacromial impingement and identify postsurgical activity guidelines that may further reduce complication rates and improve overall outcomes.

Acknowledgments

The authors thank Anthony Cresap for his help with cadaveric testing and Todd Hullfish and Annelise Slater for their help collecting motion capture data.

Disclaimer

The authors, their immediate families, and any research foundations with which they are affiliated have not received any financial payments or other benefits from any commercial entity related to the subject of this article.

Supplementary data

Supplementary data to this article can be found online at <https://doi.org/10.1016/j.jse.2018.11.062>.

References

1. Aaron D, Shatsky J, Paredes JC, Jiang C, Parsons BO, Flatow EL. Proximal humeral fractures: internal fixation. *J Bone Joint Surg Am* 2012;94:2280-8.
2. Agudelo J, Schürmann M, Stahel P, Helwig P, Morgan SJ, Zechel W, et al. Analysis of efficacy and failure in proximal humerus fractures treated with locking plates. *J Orthop Trauma* 2007;21:676-81. <http://dx.doi.org/10.1097/BOT.0b013e31815bb09d>
3. Arciero RA, Parrino A, Bernhardson AS, Diaz-Doran V, Obopilwe E, Cote MP, et al. The effect of a combined glenoid and Hill-Sachs defect on glenohumeral stability: a biomechanical cadaveric study using 3-dimensional modeling of 142 patients. *Am J Sports Med* 2015;43:1422-9. <http://dx.doi.org/10.1177/0363546515574677>
4. Badman BL, Mighell M. Fixed-angle locked plating of two-, three-, and four-part proximal humerus fractures. *J Am Acad Orthop Surg* 2008;16:294-302. <http://dx.doi.org/10.5435/00124635-200805000-00008>
5. Brunner F, Sommer C, Bahr C, Heuwinkel RM, Hafner CM, Rillmann PM, et al. Open reduction and internal fixation of proximal humerus fractures using a proximal humeral locked plate: a prospective multicenter analysis. *J Orthop Trauma* 2009;23:163-72. <http://dx.doi.org/10.1097/BOT.0b013e3181920e5b>
6. Büchler P, Ramaniraka NA, Rakotomanana LR, Iannotti JP, Farron A. A finite element model of the shoulder: application to the comparison of normal and osteoarthritic joints. *Clin Biomech (Bristol, Avon)* 2002;17:630-9. [http://dx.doi.org/10.1016/S0268-0033\(02\)00106-7](http://dx.doi.org/10.1016/S0268-0033(02)00106-7)
7. Cereatti A, Calderone M, Buckland DM, Buettner A, Della Croce U, Rosso C. In vivo glenohumeral translation under anterior loading in an open-MRI set-up. *J Biomech* 2014;47:3771-5. <http://dx.doi.org/10.1016/j.jbiomech.2014.09.021>
8. Clavert P, Adam P, Bevoit A, Bonnet F, Kempf JF. Pitfalls and complications with locking plate for proximal humerus fracture. *J Shoulder Elbow Surg* 2010;19:489-94. <http://dx.doi.org/10.1016/j.jse.2009.09.005>
9. Delp SL, Anderson FC, Arnold AS, Loan P, Habib A, John CT, et al. OpenSim: open-source software to create and analyze dynamic simulations of movement. *IEEE Trans Biomed Eng* 2007;54:1940-50. <http://dx.doi.org/10.1109/TBME.2007.901024>
10. DePuy Synthes. 3.5 mm LCP Proximal Humerus Plates Surgical Technique, <http://synthes.vo.llnwd.net/o16/LLNWMB8/US%20Mobile/Synthes%20North%20America/Product%20Support%20Materials/Technique%20Guides/DSUSTRM10161133_ProxHumPI_STG_150dpi.pdf>; 2017, accessed July 12, 2018.
11. Faraj D, Kooistra BW, Vd Stappen WA, Werre AJ. Results of 131 consecutive operated patients with a displaced proximal humerus fracture: an analysis with more than two years follow-up. *Eur J Orthop Surg Traumatol* 2011;21:7-12. <http://dx.doi.org/10.1007/s00590-010-0655-z>
12. Gordon CC, Churchill T, Clauser CE, Bradtmiller B, McConville JT. Anthropometric survey of U.S. Army Personnel: methods and summary statistics 1988. Yellow Springs, OH: Anthropology Research Project Inc <<http://www.dtic.mil/docs/citations/ADA225094>>, 1989, accessed November 8, 2018.
13. Graichen H, Bonel H, Stammberger T, Englmeier KH, Reiser M, Eckstein F. Sex-specific differences of subacromial space width during abduction, with and without muscular activity, and correlation with anthropometric variables. *J Shoulder Elbow Surg* 2001;10:129-35.
14. Graichen H, Bonel H, Stammberger T, Haubner M, Rohrer H, Englmeier KH, et al. Three-dimensional analysis of the width of the subacromial space in healthy subjects and patients with impingement syndrome. *AJR Am J Roentgenol* 1999;172:1081-6.
15. Graichen H, Bonel H, Stammberger T, Heuck A, Englmeier KH, Reiser M, et al. A technique for determining the spatial relationship between the rotator cuff and the subacromial space in arm abduction using MRI and 3D image processing. *Magn Reson Med* 1998;40:640-3.
16. Hast MW, Schmidt EC, Kelly JD, Baxter JR. Computational optimization of graft tension in simulated superior capsule reconstructions. *J Orthop Res* 2018;36:2789-96. <http://dx.doi.org/10.1002/jor.24050>
17. Holzbaur KR, Murray WM, Delp SL. A model of the upper extremity for simulating musculoskeletal surgery and analyzing neuromuscular control. *Ann Biomed Eng* 2005;33:829-40. <http://dx.doi.org/10.1007/s10439-005-3320-7>
18. Hsu JE, Russ SM, Somerson JS, Tang A, Warme WJ, Matsen FA 3rd. Is the Simple Shoulder Test a valid outcome instrument for shoulder arthroplasty? *J Shoulder Elbow Surg* 2017;26:1693-700. <http://dx.doi.org/10.1016/j.jse.2017.03.029>
19. Huffman GR, Tibone JE, McGarry MH, Phipps BM, Lee YS, Lee TQ. Path of glenohumeral articulation throughout the rotational range of motion in a Thrower's shoulder model. *Am J Sports Med* 2006;34:1662-9. <http://dx.doi.org/10.1177/0363546506287740>
20. Hughes PC, Green RA, Taylor NF. Measurement of subacromial impingement of the rotator cuff. *J Sci Med Sport* 2012;15:2-7. <http://dx.doi.org/10.1016/j.jsams.2011.07.001>
21. Kirchhoff C, Braunstein V, Kirchhoff S, Sprecher CM, Ockert B, Fischer F, et al. Outcome analysis following removal of locking plate fixation of the proximal humerus. *BMC Musculoskelet Disord* 2008;9:138. <http://dx.doi.org/10.1186/1471-2474-9-138>
22. Lee SH, Dargent-Molina P, Bréart G. Risk factors for fractures of the proximal humerus: results from the EPIDOS Prospective Study. *J Bone Miner Res* 2002;17:817-25. <http://dx.doi.org/10.1359/jbmr.2002.17.5.817>
23. Leggin BG, Michener LA, Shaffer MA, Brennehan SK, Iannotti JP, Williams GR Jr. The Penn shoulder score: reliability and validity. *J Orthop Sports Phys Ther* 2006;36:138-51. <http://dx.doi.org/10.2519/jospt.2006.36.3.138>
24. Li X, Xu W, Hu N, Liang X, Huang W, Jiang D, et al. Relationship between acromial morphological variation and subacromial impingement: a three-dimensional analysis. *PLoS One* 2017;12:e0176193. <http://dx.doi.org/10.1371/journal.pone.0176193>
25. Michener LA, McClure PW, Karduna AR. Anatomical and biomechanical mechanisms of subacromial impingement syndrome. *Clin Biomech (Bristol, Avon)* 2003;18:369-79.
26. Namdari S, Yagnik G, Ebaugh DD, Nagda S, Ramsey ML, Williams GR Jr, et al. Defining functional shoulder range of motion for activities of daily living. *J Shoulder Elbow Surg* 2012;21:1177-83. <http://dx.doi.org/10.1016/j.jse.2011.07.032>
27. Orr TE, Carter DR. Stress analyses of joint arthroplasty in the proximal humerus. *J Orthop Res* 1985;3:360-71.
28. Richards RR, An KN, Bigliani LU, Friedman RJ, Gartsman GM, Gristina AG, et al. A standardized method for the assessment of shoulder function. *J Shoulder Elbow Surg* 1994;3:347-52.
29. Saul KR, Hu X, Goehler CM, Vidt ME, Daly M, Velisar A, et al. Benchmarking of dynamic simulation predictions in two software platforms using an upper limb musculoskeletal model. *Comput Methods Biomech Biomed Engin* 2015;18:1445-58. <http://dx.doi.org/10.1080/10255842.2014.916698>
30. Schliemann B, Siemoneit J, Theisen C, Kösters C, Weimann A, Raschke MJ. Complex fractures of the proximal humerus in the elderly—outcome and complications after locking plate fixation. *Musculoskelet Surg* 2012;96:3-11. <http://dx.doi.org/10.1007/s12306-012-0181-8>
31. Seeley DG, Browner WS, Nevitt MC, Genant HK, Scott JC, Cummings SR, et al. Which fractures are associated with low appendicular bone mass in elderly women? *Ann Intern Med* 1991;115:837-42.
32. Sudkamp N, Bayer J, Hepp P, Voigt C, Oestern H, Kaab M, et al. Open reduction and internal fixation of proximal humeral fractures with use of the locking proximal humerus plate: results of a prospective,

- multicenter, observational study. *J Bone Joint Surg Am* 2009;91:1320-8. <http://dx.doi.org/10.2106/JBJS.H.00006>
33. Tasaki A, Nimura A, Nozaki T, Yamakawa A, Niitsu M, Morita W, et al. Quantitative and qualitative analyses of subacromial impingement by kinematic open MRI. *Knee Surg Sports Traumatol Arthrosc* 2015;23:1489-97. <http://dx.doi.org/10.1007/s00167-014-2876-x>
34. Thanasis C, Kontakis G, Angoules A, Limb D, Giannoudis P. Treatment of proximal humerus fractures with locking plates: a systematic review. *J Shoulder Elbow Surg* 2009;18:837-44. <http://dx.doi.org/10.1016/j.jse.2009.06.004>
35. Yang P, Zhang Y, Liu J, Xiao J, Ma LM, Zhu CR. Biomechanical effect of medial cortical support and medial screw support on locking plate fixation in proximal humeral fractures with a medial gap: a finite element analysis. *Acta Orthop Traumatol Turc* 2015;49:203-9. <http://dx.doi.org/10.3944/AOTT.2015.14.0204>